Microchemical Journal 154 (2020) 104642

Contents lists available at ScienceDirect

Microchemical Journal

journal homepage: www.elsevier.com/locate/microc

In situ formation of Ag/Au nanorods as a platform to design a non-aggregation colorimetric assay for uric acid detection in biological fluids

Mohammad Amjadi[a,*], Tooba Hallaj[a,b], Elham Nasirloo[a]

[a] Department of Analytical Chemistry, Faculty of Chemistry, University of Tabriz, Tabriz 5166616471, Iran
[b] Cellular and Molecular Research Center, Cellular and Molecular Medicine Institute, Urmia University of Medical Sciences, Urmia, Iran

ARTICLE INFO

Keywords:
Uric acid
Surface plasmon resonance
Au nanorods
Sensor

ABSTRACT

Herein, we report on a sensitive probe for colorimetric detection of uric acid based on the formation of Ag shell on Au nanorods (Ag/AuNRs) in the presence of uric acid. Uric acid can reduce Ag^+ to Ag atoms which deposit on the surface of AuNRs and form Ag shell. As a result of this phenomenon, the dielectric environment around AuNRs changes and the longitudinal surface plasmon resonance (SPR) peak of AuNRs blue-shifts, leading to the change of solution color from purple to green. Based on these facts, a colorimetric sensor for the detection of uric acid in the concentration range of 0.1–1.0 μM with a detection limit of 0.065 μM was developed. The method was applied for analysis of uric acid in human plasma and urine samples with satisfactory results. The sensor can be used for uric acid detection even with bare eyes.

1. Introduction

Uric acid (2,6,8-trihydroxypurine) is the main product of the catabolism of the purine nucleosides, adenosine and guanosine. Besides, purines from catabolism of dietary nucleic acid are directly converted to uric acid. Most purine metabolism disorders stem from both hypouricemias and hyperuricemias. When the concentration of uric acid in plasma is greater than 7.0 mg/dL (0.42 mM) in men or greater than 6.0 mg/dL (0.36 mM) in women, hyperuricemia occurs. In clinical diagnosis, the plasma uric acid level is usually monitored for the investigation of gout, either as a result of primary hyperuricemia or caused by other conditions or treatments that give rise to secondary hyperuricemias. This analysis is also applied for examination of pregnancy-induced hypertension [1].

Several methods have been reported for the detection of uric acid such as fluorescence [2–4] chromatography [5–7], electrochemical methods [8–10], colorimetric assays and so on [11–20]. Among these, colorimetric methods have advantages including rapidness, low cost and simplicity in monitoring (even with naked eyes) for determination of different species [21,22]. Recently, several colorimetric methods have been designed based on noble metal nanoparticles with different shapes, such as spherical nanoparticles (NPs) [23,24], nanostars [25], nanopyramids [26] and nanorods [27,28], due to their strong localized surface plasmon resonance (LSPR) peak in the visible region. LSPR stems from the interaction of the incident light with conduction electrons of the metal NPs, which produces the coherent localized plasmon oscillations with a resonant frequency. A variety of parameters such as the size, shape, composition, dielectric environment, and distance between NPs can influence on the intensity and frequency of the plasmonic band [29]. Even though, the aggregation-based colorimetric methods [22] have been developed much more than the non-aggregation based methods, nowadays the non-aggregation based sensors, including those based on NP etching and growth, are also received tremendous attention [21,30–33]. Anisotropic and bimetallic NPs are more suitable for designing these kinds of sensors. Colorimetric probes based on the gold nanorod (AuNRs), which have two LSPR bands, indicate sharp color changes, so can be applied for sensitive determinations. This fact results from the tunable longitudinal LSPR band from the visible to NIR region which is obtained via varying the aspect ratios of NRs [29]. Moreover, bimetallic nanoparticles including silver-coated gold nanorods (Ag/AuNRs) can be applied as a substantial choice for designing colorimetric methods because with changing the Ag shell thickness around AuNRs, as a result of its growing [34–37] or etching [38–40], the LSPR peak shifts and distinctive colors appear. However, the colorimetric sensors based on the transformation AuNRs, despite of their high potential to detect various species with high sensitivity and selectivity, have rarely been reported.

Herein, we designed an enzyme-free colorimetric probe for the determination of uric acid based on growing Ag nanoshell on the AuNRs and applied it for monitoring uric acid in biological samples with

* Corresponding author.
E-mail address: amjadi@tabrizu.ac.ir (M. Amjadi).

https://doi.org/10.1016/j.microc.2020.104642
Received 31 October 2019; Received in revised form 16 December 2019; Accepted 13 January 2020
Available online 14 January 2020
0026-265X/

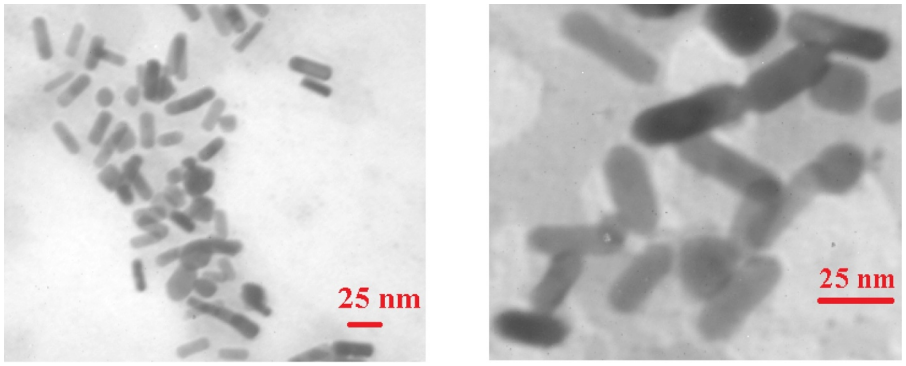

Fig. 1. TEM image of (a) AuNRs and (b) Ag/AuNRs.

satisfactory results. This is a non-aggregation colorimetric probe in which wavelength-variation sensing strategy was used for detection of uric acid. This feature makes our method robust and suitable for biological analysis.

2. Experimental

2.1. Materials

Analytical reagent-grade chemicals were used throughout. Solutions were prepared with ultra-pure water obtained from aqua MAX - Ultra 370 water purification system (Young Lin Instrument Co., Korea). Gold (III) chloride trihytrate ($HAuCl_4 \cdot 3H_2O$), glycine, sodium borohydride ($NaBH_4$), ascorbic acid and silver nitrate ($AgNO_3$) were purchased from Merck (Darmstadt, Germany). Cetyltrimethylammonium bromide (CTAB) was obtained from Sigma. A uric acid stock solution was prepared by dissolving an appropriate amount of uric acid (Merck) in a minimum volume of 3 M sodium hydroxide (NaOH) and deionized water.

2.2. Apparatus

UV–Vis absorption spectra were recorded on a Carry-100 double-beam UV–Vis spectrophotometer with 1.0 cm quartz cells. Nanorods were characterized by transmission electron microscopy (TEM, Philips CM120, operated at 430 kV) and X-ray powder diffraction (XRD) patterns (measured by a Siemens D 500 instrument, Germany).

2.3. Synthesis of AuNRs

AuNRs were synthesized by a method reported by Nikoobakht and El-Sayed [41]. At first, the Au seed solution (small spherical AuNPs) was prepared by adding CTAB (2.5 mL, 0.2 M) to $HAuCl_4$ solution (2.5 mL, 0.5 mM), and then adding the freshly prepared $NaBH_4$ solution (30 μL, 0.1 M) and vigorously stirring the mixture for 2 min. The color of the obtained seed solution was yellowish-brown. This solution was aged for 2 h before use. The growth solution including CTAB (5.0 mL, 0.2 M), $HAuCl_4$ (4.0 mL, 0.001 M) and $AgNO_3$ (60 mL, 0.004 M) was also prepared by adding ascorbic acid (70 μL, 0.0788 M) with slowly stirring. At last, 15 μL of Au seed was added to the growth solution and the obtained mixture was incubated for 2 h at 37 °C.

2.4. General procedure for the determination of uric acid

50 μL of the prepared AuNRs was mixed with 50 μL of glycine buffer solution (pH = 9.5, 0.1 M) in the centrifuge tube. Subsequently, different concentration of uric acid standard or sample solution was added to the mixture. Then, 10 μL of $AgNO_3$ (0.01 M) was also added and the final volume was adjusted to 1.0 mL with ultrapure water. After incubation at 40 °C for 2 min, the absorption spectrum of colloid solution was recorded by spectrophotometer over the range of 400–900 nm.

2.5. Preparation of biological samples

To precipitate the plasma proteins, 2.0 mL acetonitrile was added to 500 μL of human plasma sample into a centrifuge tube. The obtained mixture was centrifuged for 15 min at 4000 rpm. Then, the supernatant was transferred into a 5.0-mL volumetric flask and diluted to the mark with ultrapure water. A suitable amount of this solution was taken for analysis according to the general procedure.

For urine samples, 100 μL of urine was transferred into a 100-mL volumetric flask and diluted to the mark with ultrapure water. A suitable amount of this solution was taken for analysis according to the general procedure.

3. Results and discussion

The prepared AuNRs were characterized by TEM image and UV–Vis absorption spectra. As shown in Fig. 1(a), the average diameter and length of AuNRs were 8 nm and 25 nm, respectively. The absorption spectrum of AuNRs (Fig. 2) exhibited two characteristic peaks around 525 nm and 740 nm, corresponding to the transverse and longitudinal plasmon oscillations, respectively.

3.1. Colorimetric assay

Our investigations indicated that in the presence of Ag^+ and uric acid as reducing agent, the color of AuNR solution changes from purple to green and AuNR LSPR peak at 740 nm shifts to lower wavelengths while no significant variation is observed in the position of the second peak (525 nm). Uric acid (with redox potential of 0.47 V vs NHS at pH ~ 9 [42]) can reduce Ag^+ (with redox potential of 0.799 V) to Ag^0 which deposits on the surface of AuNRs [34,35]. So, AuNRs are converted into Ag/Au core-shell NRs. To confirm this assertion, we compared TEM images of AuNRs in the presence and absence of uric acid and Ag^+. As can be seen in Fig. 1, the average diameter and length of AuNRs in the presence of uric acid and Ag^+ increased considerably. The calculation of aspect ratio of NRs in the absence and presence of uric acid indicated that in the presence of uric acid aspect ratio reduces from 3.1 to 2.5. This change can be attributed to the fact that Ag atoms tend to deposit on the longer side of NRs [34]. To further confirm the formation of Ag shell, we used its reaction with nitric acid. It is known that nitric acid can just dissolve Ag shell but barely affect Au core [43]. Therefore, the effect of nitric acid was investigated on both AuNRs and Ag/AuNRs. As shown in Fig. S1 (Electronic Supplementary Material), the LSPR band of Ag/AuNRs red-shifted upon reaction with nitric acid

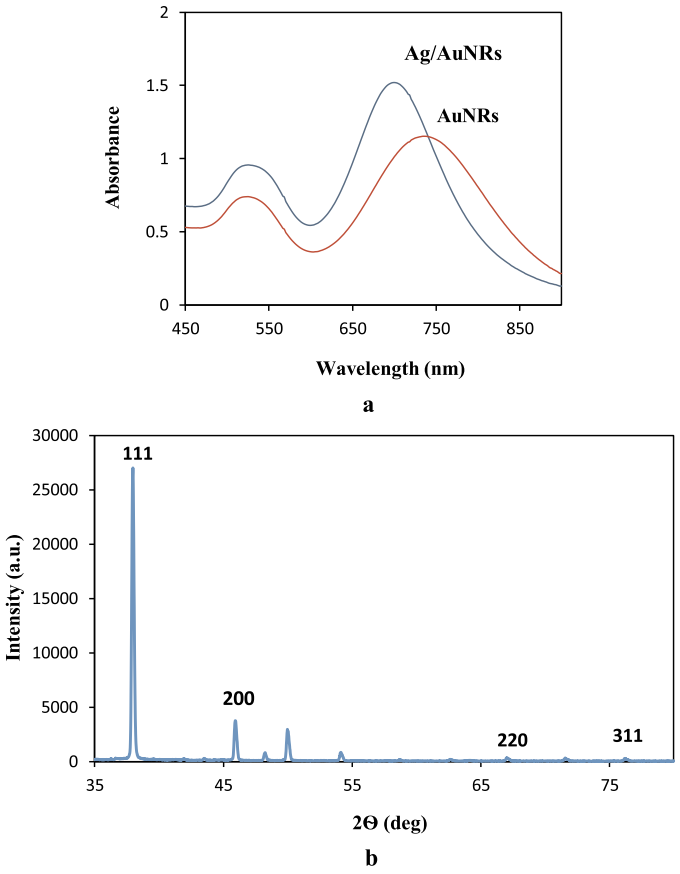

Fig. 2. (a) Absorption spectra of AuNRs in the absence and presence of uric acid. *Conditions:* buffer (5 mM, pH = 9.5), $AgNO_3$ (0.1 mM), AuNRs volume (50 μL), temperature (40 °C), time (2 min) and uric acid 0.5 μM. (b) XRD pattern of Ag/AuNRs.

while no significant change was observed for LSPR peak of AuNRs. This evidence verified that changes in the shape and aspect ratio of AuNRs are related to the formation of Ag shell on AuNRs. Moreover, the characteristic peaks of crystalline (111), (200), (220), and (311) planes of Au and Ag (JCPDS file Nos. 01–1174 and 04–0783, respectively) can be observed in the recorded XRD pattern (Fig. 2(b)). According to the literature, due to the small mismatch in the lattices of Au and Ag crystals, no clear difference can be observed between Au and Ag diffraction angles in the XRD patterns of the Ag/Au core/shell nanostructures [44]. It should be mentioned that with increasing the concentration of uric acid, the thickness of Ag layer on the AuNRs increases, resulting in greater change in the dielectric environment around AuNRs. As a result, the blue-shift for the LSPR peak at 740 nm increases. The variation in the LSPR peak position and solution color is proportional to the concentration of uric acid. Based on these facts, we designed a colorimetric sensor for detection of uric acid in biological samples. The overall principle of this sensor is shown in Scheme 1.

3.2. Optimization of assay conditions

In order to obtain the highest sensitivity for the assay, the effect of parameters such as pH, buffer concentration, concentration of $AgNO_3$, amount of AuNRs, the reaction temperature and time was examined on the analytical signal. The wavelength variation of AuNRs/ Ag^+ in the absence and presence of uric acid was applied as an analytical signal ($\Delta\lambda = \lambda_0 - \lambda$, where λ and λ_0 represent the absorption wavelength in the absence and presence of uric acid, respectively).

Since the reducing property of uric acid is improved in the alkaline condition [45], the effect of pH of solution on the $\Delta\lambda$ was studied in the range of 8.0–10.5. The glycine buffer was used for pH adjustment because glycine can form a complex with Ag^+ which keeps it from participation with ions such as Cl^-, Br^-, OH^- and so on. On the other hand, since the charge of Ag^+-glycine complex is negative, it can readily adsorb on the surface of AuNRs with positive charge and facilitate the reduction of Ag^+ to Ag^0 on the surface of AuNRs [46]. As indicated in Fig. 3(A), the highest signal was obtained at pH = 9.5. Due to the formation of AgOH as well as aggregation of AuNRs, the $\Delta\lambda$ decreased at higher pH. The concentration of glycine was also optimized. As can be seen in Fig. 3(B), the maximum signal was obtained for 0.005 M glycine.

We also investigated the influence of the $AgNO_3$ concentration in the range of 0.01- 0.5 mM on the $\Delta\lambda$ of colorimetric system (Fig. 3(C)). According to the results, the maximum signal was achieved with 0.1 mM, so this amount was chosen as the optimum concentration of $AgNO_3$ for the next experiments. With the increasing Ag^+ concentration up to 0.1 mM the formation of Ag atoms increases and the thickness of Ag layer on the AuNRs will also increase, resulting in an increase in $\Delta\lambda$. However, at higher concentrations of Ag^+, AgNPs (with SPR peak around 400 nm) can also form and aggregate [47], so the analytical signal was not favorable.

The other parameter which its effect on $\Delta\lambda$ was examined is the amount of AuNRs. As can be seen in Fig. 3(D), the analytical signal is improved by decreasing the volume of AuNRs from 200 to 25 μL. However, in the volumes less than 50 μL, the absorbance intensity sharply dropped, so the $\Delta\lambda$ measurement was difficult. Therefore, 50 μL was chosen as the optimal volume in this study.

The influence of the reaction temperature on the $\Delta\lambda$ was also studied (Fig. 3(E)). No variation in the wavelength was observed at ambient temperature which indicated that the reduction of Ag^+ by uric acid on the AuNR surface could not take place without heat. The highest $\Delta\lambda$ was achieved at 40 °C. Decreasing in the signal at higher temperatures can be attributed to the formation of AgNPs and deformation of AuNRs.

Finally, the effect of incubation time on the formation of Ag/AuNRs was investigated at three concentrations of uric acid (Fig. 3(F)). We observed that with increasing the incubation time, λ_0 shifted to the lower wavelength which resulted in the diminution of $\Delta\lambda$. It can be attributed to the reducing effect of ascorbic acid remained in the prepared AuNRs which can reduce Ag^+ to Ag^0 [34,35]. Therefore, the incubation time of 2 min was applied for further experiments.

3.3. Analytical performance of the colorimetric sensor

Under the mentioned optimum conditions, the effect of uric acid concentration was studied on the signaling of designed sensor. With increasing the concentration of uric acid, the reduction of Ag^+ to Ag^0 and so the thickness of the formed Ag shell on the AuNRs increased. As a result of this phenomenon, the longitudinal LSPR peak of AuNRs blue-shifted and the color of the solution changed from purple to green (Fig. 4(a)). The wavelength variation was proportional to the uric acid concentration. We found a linear relationship between the uric acid concentration and $\Delta\lambda$ in the range of 0.1–1.0 μM with a detection limit of 0.065 μM. The regression equation is $\Delta\lambda = 22.11C + 16.11$ ($R^2 = 0.9985$), where $\Delta\lambda = \lambda_0 - \lambda$ is the difference between the wavelength of LSRP peak of AuNRs in the presence of uric acid (λ) and its absence (λ_0), and C is the concentration of uric acid in μM. The relative standard deviation (RSD) was 2.7% for five replicate measurements of uric acid.

To evaluate the selectivity of sensor, the effect of various species, including ions and biomolecules which can be found in biological fluids, was studied on the determination of uric acid. The tolerance limits for interfering species in the relative error of < 5% are presented in Table 1. Most remarkable interference effects were observed for ascorbic acid, glutathione, and cysteine. But the normal concentrations of these species in plasma are respectively lower than 70 [48], 0.5 [49],

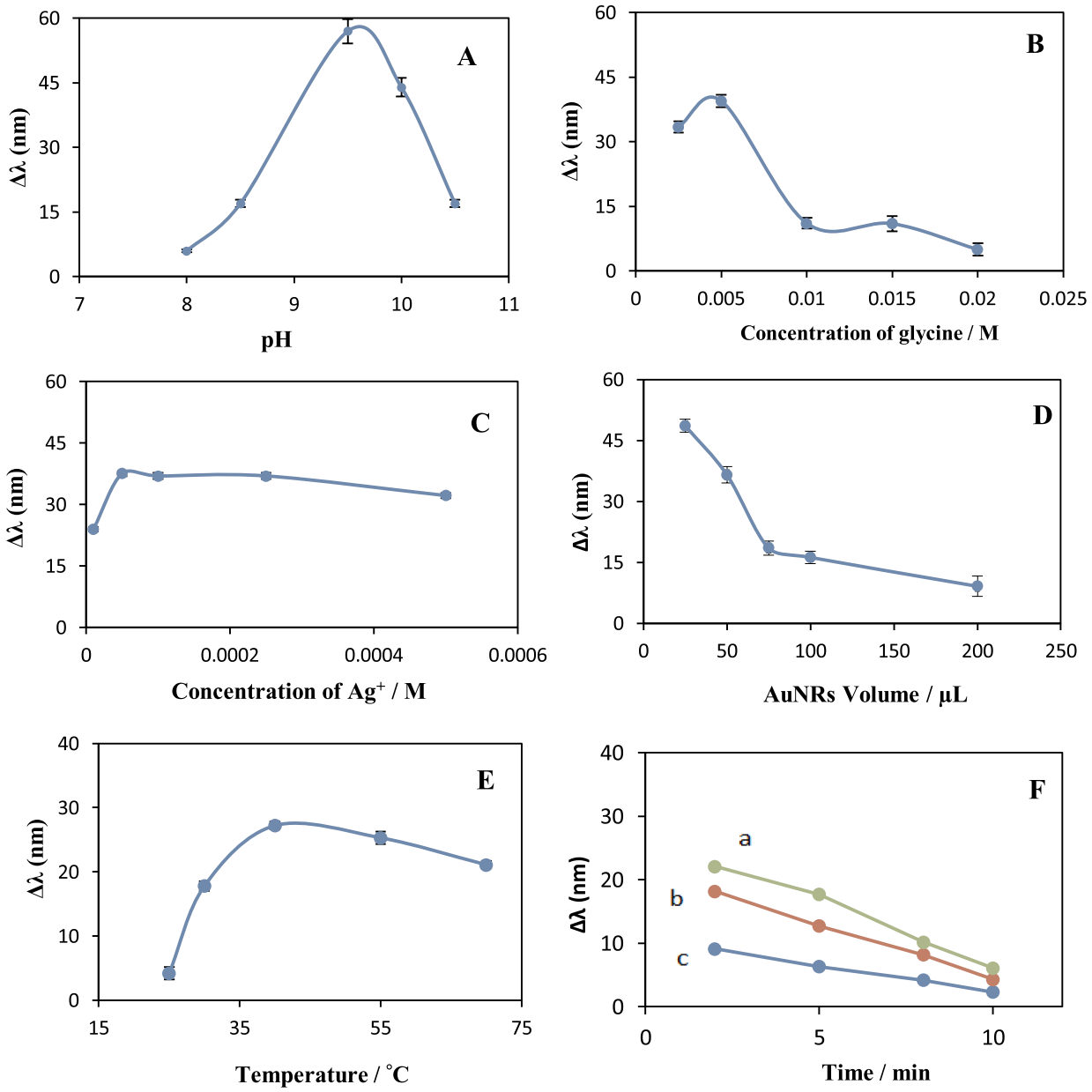

Fig. 3. Optimization of experimental parameters. (A) Effect of pH; *condition:* $AgNO_3$ (0.1 mM), AuNRs volume (50 µL), temperature (40 °C), time (2 min) and uric acid 1 µM. (B) Effect of glycine concentration; pH (9.5), other conditions are as in A. (C) Effect of the $AgNO_3$ concentration; glycine concentration (0.005 M), other conditions are as in B. (D) Effect of Au NRs volume; *conditions:* $AgNO_3$ (0.1 mM), other conditions are as in C. (E) Effect of reaction temperature on the Δλ system; *conditions:* AuNRs (50 µL) uric acid 0.5 µM, other conditions are as in D. (F) Effect of reaction time (a) 1.0 µM (b) 0.5 µM (c) 0.1 µM of uric acid; *conditions:* temperature (40 °C) other conditions are as in E.

250 µM [50], which are lower than the normal plasma concentration of uric acid. Moreover, the final concentrations of these species are below their tolerance limits in our method. Glucose is another species with relatively high concentration in plasma (around 7 mM in normal person [51]), but it is much lower than the tolerance limit of our method. Therefore, none of these species interferes with uric acid determination. These results confirmed the suitable selectivity of the method for analysis of biological samples.

We also compared our developed method with some other previously reported methods (Table 2). The detection limit of this method is comparable or superior to that of others. Furthermore, the synthesis of AuNRs compared to the nanoparticles applied in other methods is simpler and less time-consuming.

3.4. Analytical application

In order to investigate the applicability of the sensor for monitoring uric acid in biological samples, we exploited it to measure uric acid levels in the human plasma and urine samples. The results are reported in Table 3. Moreover, the analysis of uric acid in spiked samples was applied to evaluate the accuracy of the introduced method. Statistical analysis of the obtained data by Student *t*-test indicated that there is no significant difference between the found and added uric acid amounts in the spiked samples, which confirmed the accuracy of the method.

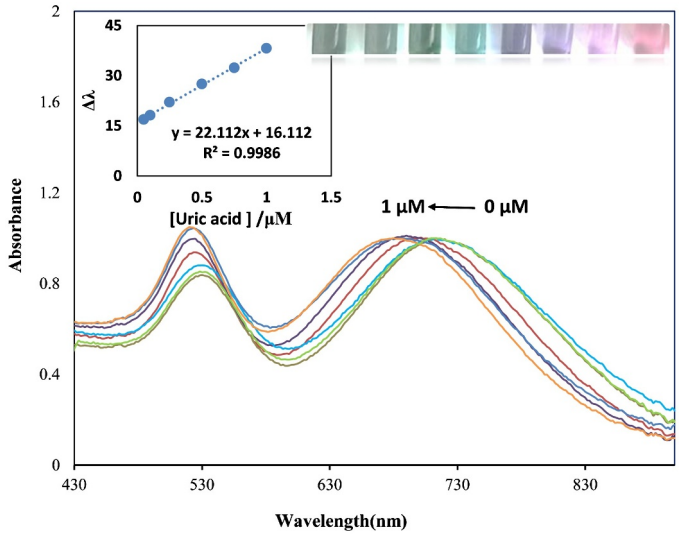

Fig. 4. (a) UV–vis absorption spectra of AuNRs-Ag^+ with different concentration of uric acid; b) calibration curve for uric acid. Conditions: pH = 9.5 (buffer, 5.0 mM), AuNRs (50 μL), $AgNO_3$ (0.1 mM), time (2 min) and T = 40°C.

4. Conclusions

In summary, a wavelength-variation colorimetric sensor was designed for the detection of uric acid based on the formation of Ag shell on AuNRs. Ag^+ is reduced to Ag^0 by uric acid, and the formed Ag^0 deposits on the AuNRs which leads to the formation of Ag/AuNRs. As a result, a blue-shift is observed in longitudinal LSPR band of AuNRs and the color of the solution changes from purple to green. With increasing the concentration of uric acid, the amount of blue-shift and solution color variation increases. Based on these facts, a simple and sensitive colorimetric method was developed for detection of uric acid in biological samples.

Table 1
Tolerance limits of interferences in the determination of 0.5 μM uric acid.

Interfering species	Tolerance limit
Inorganic species	
NO_3^-, Mg^{2+}, K^+, Na^+	1000
SO_4^{2-}, Zn^{2+}, Cl^-	500
PO_4^{3-}, Ca^{2+}	100
Cu^{2+}	15
Fe^{3+}	10
Organic species	
Glycine, Lactose	1000
α-Alanine, Tryptophan, Sucrose	500
Glucose	125
Ascorbic acid, Glutathione, Cysteine	5

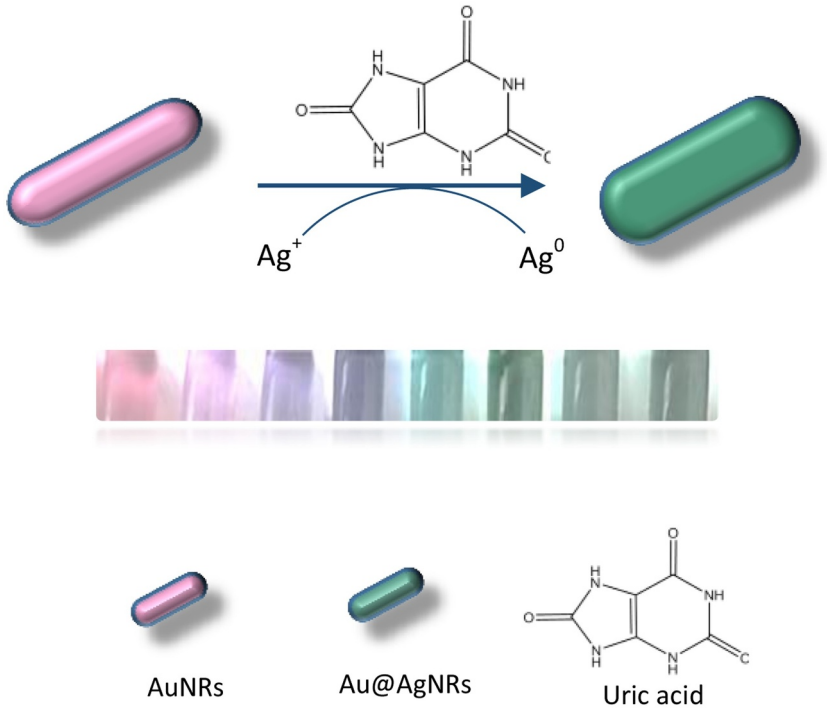

Scheme 1. Principle of the developed sensor for uric acid.

Table 2
Comparison of the developed method with some other colorimetric methods for determination of uric acid.

Colorimetric Method	Linear range (M)	LOD (M)	Ref
Th-MOF-based method	$4 \times 10^{-6}$to 7×10^{-5}	1.15×10^{-6}	[11]
MIP-NP-based method	$2.97 \times 10^{-6}$to 2.37×10^{-4}	1.46×10^{-6}	[12]
Upconversion NP-based method	$1 \times 10^{-5}$to 1×10^{-3}	5.79×10^{-6}	[13]
Heme-ficin complex-based method	$1 \times 10^{-6}$to 12×10^{-5}	2.5×10^{-7}	[14]
Cu^{2+}- TMB–H_2O_2-based method	1×10^{-6} to 1×10^{-4}	6.4×10^{-7}	[15]
Ag nanoprism-based method	1.0×10^{-6} to 4.0×10^{-5}	7.0×10^{-7}	[16]
Unmodified Ag nanoprism-based method	1.0×10^{-8} to 3×10^{-6}	1.0×10^{-8}	[17]
AuNP-based method	5.0×10^{-7} to 4.0×10^{-6}	5.0×10^{-7}	[18]
Ag@Au NR-based method	$1.0 \times 10^{-7}$to 1×10^{-6}	6.5×10^{-8}	This work

Table 3
Determination of uric acid in human plasma and urine Samples.

Sample	Added (mM)	Found (mM)	Recovery (%)[a]	*t*-statistic[b]
Plasma1	0.0	0.162 ± 0.001	–	–
	0.1	0.260 ± 0.005	99 ± 6	0.6
	0.2	0.36 ± 0.01	97 ± 5	0.83
Plasma2	0.0	0.195 ± 0.001	–	–
	0.1	0.298 ± 0.004	103 ± 4	1.24
	0.2	0.392 ± 0.008	98 ± 4	0.61
Urine1	0.0	1.20 ± 0.001	–	–
	0.3	1.49 ± 0.01	96 ± 5	1.37
	0.5	1.69 ± 0.02	98 ± 5	0.72
Urine2	0.0	1.430 ± 0.001	–	–
	0.3	1.71 ± 0.01	93 ± 4	2.72
	0.5	1.92 ± 0.02	98 ± 5	0.75

[a] Mean of three determinations ± standard deviation.
[b] t-Critical = 4.3 for $n = 2$ and $P = 0.05$.

CRediT authorship contribution statement

Mohammad Amjadi: Conceptualization, Supervision, Resources, Writing - review & editing. **Tooba Hallaj:** Methodology, Formal analysis, Writing - original draft. **Elham Nasirloo:** Investigation, Validation, Writing - original draft.

Declaration of Competing Interest

The authors declare that they have no known competing financial interests or personal relationships that could have appeared to influence the work reported in this paper.

Supplementary materials

Supplementary material associated with this article can be found, in the online version, at doi:10.1016/j.microc.2020.104642.

References

[1] C.A. Burtis, E.R. Ashwood, D.E. Bruns, N.W. Tietz (Eds.), Tietz Textbook of Clinical Chemistry and Molecular Diagnostics: With 12 Color Plates, 4th ed, Elsevier, Saunders, St. Louis, MO, 2006.

[2] N.E. Azmi, N.I. Ramli, J. Abdullah, M.A. Abdul Hamid, H. Sidek, S. Abd Rahman, N. Ariffin, N.A. Yusof, A simple and sensitive fluorescence based biosensor for the determination of uric acid using H_2O_2-sensitive quantum dots/dual enzymes, Biosens. Bioelectron. 67 (2015) 129–133, https://doi.org/10.1016/j.bios.2014.07.056.

[3] R.-M. Kong, A. Yang, Q. Wang, Y. Wang, L. Ma, F. Qu, Uricase based fluorometric determination of uric acid based on the use of graphene quantum dot@silver core-shell nanocomposites, Microchim. Acta 185 (2018), https://doi.org/10.1007/s00604-017-2614-4.

[4] Y. Zhou, B. Ling, H. Chen, L. Wang, Mn^{2+}-doped NaYF4:Yb,Er upconversion nanoparticles for detection of uric acid based on the Fenton reaction, Talanta 180 (2018) 120–126, https://doi.org/10.1016/j.talanta.2017.12.016.

[5] Y. Zuo, Y. Yang, Z. Zhu, W. He, Z. Aydin, Determination of uric acid and creatinine in human urine using hydrophilic interaction chromatography, Talanta 83 (2011) 1707–1710, https://doi.org/10.1016/j.talanta.2010.11.073.

[6] S.K. George, M.T. Dipu, U.R. Mehra, P. Singh, A.K. Verma, J.S. Ramgaokar, Improved HPLC method for the simultaneous determination of allantoin, uric acid and creatinine in cattle urine, J. Chromatogr. B 832 (2006) 134–137, https://doi.org/10.1016/j.jchromb.2005.10.051.

[7] N. Wijemanne, P. Soysa, S. Wijesundara, H. Perera, Development and validation of a simple high performance liquid chromatography/UV method for simultaneous determination of urinary uric acid, hypoxanthine, and creatinine in human urine, Int. J. Anal. Chem. 2018 (2018) 1–6, https://doi.org/10.1155/2018/1647923.

[8] Z.-H. Sheng, X.-Q. Zheng, J.-Y. Xu, W.-J. Bao, F.-B. Wang, X.-H. Xia, Electrochemical sensor based on nitrogen doped graphene: simultaneous determination of ascorbic acid, dopamine and uric acid, Biosens. Bioelectron. 34 (2012) 125–131, https://doi.org/10.1016/j.bios.2012.01.030.

[9] G. Wang, J. Sun, W. Zhang, S. Jiao, B. Fang, Simultaneous determination of dopamine, uric acid and ascorbic acid with $LaFeO_3$ nanoparticles modified electrode, Microchim. Acta 164 (2009) 357–362, https://doi.org/10.1007/s00604-008-0066-6.

[10] Z. Xu, M. Zhang, H. Zou, J. Liu, D. Wang, J. Wang, L. Wang, Non-enzymatic electrochemical detection of uric acid with electrodeposited Nafion film, J. Electroanal. Chem. 841 (2019) 129–134, https://doi.org/10.1016/j.jelechem.2019.04.028.

[11] A. Badoei-dalfard, N. Sohrabi, Z. Karami, G. Sargazi, Fabrication of an efficient and sensitive colorimetric biosensor based on Uricase/Th-MOF for uric acid sensing in biological samples, Biosens. Bioelectron. 141 (2019) 111420, , https://doi.org/10.1016/j.bios.2019.111420.

[12] A. Göçenoğlu Sarıkaya, B. Osman, T. Çam, A. Denizli, Molecularly imprinted surface plasmon resonance (SPR) sensor for uric acid determination, Sens. Actuators B Chem. 251 (2017) 763–772, https://doi.org/10.1016/j.snb.2017.05.079.

[13] A. Fang, Q. Wu, Q. Lu, H. Chen, H. Li, M. Liu, Y. Zhang, S. Yao, Upconversion ratiometric fluorescence and colorimetric dual-readout assay for uric acid, Biosens. Bioelectron. 86 (2016) 664–670, https://doi.org/10.1016/j.bios.2016.07.055.

[14] Y. Pan, Y. Yang, Y. Pang, Y. Shi, Y. Long, H. Zheng, Enhancing the peroxidase-like activity of ficin via heme binding and colorimetric detection for uric acid, Talanta 185 (2018) 433–438, https://doi.org/10.1016/j.talanta.2018.04.005.

[15] H.-F. Lu, J.-Y. Li, M.-M. Zhang, D. Wu, Q.-L. Zhang, A highly selective and sensitive colorimetric uric acid biosensor based on Cu(II)-catalyzed oxidation of 3,3′,5,5′-tetramethylbenzidine, Sens. Actuators B Chem. 244 (2017) 77–83, https://doi.org/10.1016/j.snb.2016.12.127.

[16] D. Wu, H.-F. Lu, H. Xie, J. Wu, C.-M. Wang, Q.-L. Zhang, Uricase-stimulated etching of silver nanoprisms for highly selective and sensitive colorimetric detection of uric acid in human serum, Sens. Actuators B Chem. 221 (2015) 1433–1440, https://doi.org/10.1016/j.snb.2015.07.088.

[17] K. Tan, G. Yang, H. Chen, P. Shen, Y. Huang, Y. Xia, Facet dependent binding and etching: ultra-sensitive colorimetric visualization of blood uric acid by unmodified silver nanoprisms, Biosens. Bioelectron. 59 (2014) 227–232, https://doi.org/10.1016/j.bios.2014.03.048.

[18] R.K. Bera, A. Anoop, C.R. Raj, Enzyme-free colorimetric assay of serum uric acid, Chem. Commun. 47 (2011) 11498, https://doi.org/10.1039/c1cc13349g.

[19] Y. He, F. Qi, X. Niu, W. Zhang, X. Zhang, J. Pan, Uricase-free on-demand colorimetric biosensing of uric acid enabled by integrated CoP nanosheet arrays as a monolithic peroxidase mimic, Anal. Chim. Acta 1021 (2018) 113–120, https://doi.org/10.1016/j.aca.2018.02.073.

[20] X. Niu, Y. He, W. Zhang, X. Li, F. Qiu, J. Pan, Elimination of background color interference by immobilizing Prussian blue on carbon cloth: a monolithic peroxidase mimic for on-demand photometric sensing, Sens. Actuators B Chem. 256 (2018) 151–159, https://doi.org/10.1016/j.snb.2017.10.072.

[21] Z. Zhang, H. Wang, Z. Chen, X. Wang, J. Choo, L. Chen, Plasmonic colorimetric sensors based on etching and growth of noble metal nanoparticles: strategies and applications, Biosens. Bioelectron. 114 (2018) 52–65, https://doi.org/10.1016/j.bios.2018.05.015.

[22] D. Vilela, M.C. González, A. Escarpa, Sensing colorimetric approaches based on gold and silver nanoparticles aggregation: chemical creativity behind the assay: A review, Anal. Chim. Acta 751 (2012) 24–43, https://doi.org/10.1016/j.aca.2012.08.043.

[23] H.K. Sung, S.Y. Oh, C. Park, Y. Kim, Colorimetric detection of Co^{2+} ion using silver nanoparticles with spherical, plate, and rod shapes, Langmuir 29 (2013) 8978–8982, https://doi.org/10.1021/la401408f.

[24] H. Song, Z. Li, Y. Peng, X. Li, X. Xu, J. Pan, X. Niu, Enzyme-triggered in situ formation of Ag nanoparticles with oxidase-mimicking activity for amplified detection

of alkaline phosphatase activity, Analyst 144 (2019) 2416–2422, https://doi.org/10.1039/C9AN00105K.
[25] M.S. Verma, P.Z. Chen, L. Jones, F.X. Gu, Branching and size of CTAB-coated gold nanostars control the colorimetric detection of bacteria, RSC Adv. 4 (2014) 10660–10668, https://doi.org/10.1039/C3RA46194G.
[26] C. Lertvachirapaiboon, I. Kiyokawa, A. Baba, K. Shinbo, K. Kato, Colorimetric determination of hydrogen peroxide based on localized surface plasmon resonance of silver nanoprisms using a microchannel chip, Anal. Lett. 52 (2019) 1939–1950, https://doi.org/10.1080/00032719.2019.1586913.
[27] D. Li, G. Zheng, X. Ding, J. Wang, J. Liu, L. Kong, DNA functionalized gold nanorods/nanoplates assembly as sensitive LSPR-based sensor for label-free detection of mercury ions, Colloids Surf. B Biointerf. 110 (2013) 485–488, https://doi.org/10.1016/j.colsurfb.2013.04.039.
[28] Y. Wang, R. Liang, W. Liu, Q. Zhao, X. Zhu, L. Yang, P. Zou, X. Wang, F. Ding, H. Rao, A dual-mode probe for colorimetric and fluorometric detection of cysteine based on phosphorus/nitrogen co-doped CQDs and gold nanorods, Sens. Actuators B Chem. 273 (2018) 1627–1634, https://doi.org/10.1016/j.snb.2018.07.084.
[29] H. Chen, L. Shao, Q. Li, J. Wang, Gold nanorods and their plasmonic properties, Chem. Soc. Rev. 42 (2013) 2679–2724, https://doi.org/10.1039/C2CS35367A.
[30] T. Lou, L. Chen, Z. Chen, Y. Wang, L. Chen, J. Li, Colorimetric detection of trace copper ions based on catalytic leaching of silver-coated gold nanoparticles, ACS Appl. Mater. Interf. 3 (2011) 4215–4220, https://doi.org/10.1021/am2008486.
[31] R. Liu, Z. Chen, S. Wang, C. Qu, L. Chen, Z. Wang, Colorimetric sensing of copper(II) based on catalytic etching of gold nanoparticles, Talanta 112 (2013) 37–42, https://doi.org/10.1016/j.talanta.2013.01.065.
[32] S. Xu, L. Jiang, Y. Liu, P. Liu, W. Wang, X. Luo, A morphology-based ultrasensitive multicolor colorimetric assay for detection of blood glucose by enzymatic etching of plasmonic gold nanobipyramids, Anal. Chim. Acta 1071 (2019) 53–58, https://doi.org/10.1016/j.aca.2019.04.053.
[33] Y. Guo, J. Wu, J. Li, H. Ju, A plasmonic colorimetric strategy for biosensing through enzyme guided growth of silver nanoparticles on gold nanostars, Biosens. Bioelectron. 78 (2016) 267–273, https://doi.org/10.1016/j.bios.2015.11.056.
[34] M.V. Gorbunova, V.V. Apyari, S.G. Dmitrienko, A.V. Garshev, Formation of core-shell Au@Ag nanorods induced by catecholamines: a comparative study and an analytical application, Anal. Chim. Acta 936 (2016) 185–194, https://doi.org/10.1016/j.aca.2016.07.038.
[35] J.-M. Liu, X.-X. Wang, M.-L. Cui, L.-P. Lin, S.-L. Jiang, L. Jiao, L.-H. Zhang, A promising non-aggregation colorimetric sensor of AuNRs–Ag+ for determination of dopamine, Sens. Actuators B Chem. 176 (2013) 97–102, https://doi.org/10.1016/j.snb.2012.08.083.
[36] T. Lin, Z. Li, Z. Song, H. Chen, L. Guo, F. Fu, Z. Wu, Visual and colorimetric detection of p-aminophenol in environmental water and human urine samples based on anisotropic growth of Ag nanoshells on Au nanorods, Talanta 148 (2016) 62–68, https://doi.org/10.1016/j.talanta.2015.10.056.
[37] Y. Wang, Y. Zeng, W. Fu, P. Zhang, L. Li, C. Ye, L. Yu, X. Zhu, S. Zhao, Seed-mediated growth of Au@Ag core-shell nanorods for the detection of ellagic acid in whitening cosmetics, Anal. Chim. Acta 1002 (2018) 97–104, https://doi.org/10.1016/j.aca.2017.11.067.
[38] J. Zhu, B. Zhao, Y. Qi, J.-J. Li, X. Li, J.-W. Zhao, Colorimetric determination of Hg (II) by combining the etching and aggregation effect of cysteine-modified Au–Ag core-shell nanorods, Sens. Actuators B Chem. 255 (2018) 2927–2935, https://doi.org/10.1016/j.snb.2017.09.113.
[39] Z. Chen, Z. Zhang, C. Qu, D. Pan, L. Chen, Highly sensitive label-free colorimetric sensing of nitrite based on etching of gold nanorods, Analyst 137 (2012) 5197, https://doi.org/10.1039/c2an35787a.
[40] T. Lin, M. Zhang, F. Xu, X. Wang, Z. Xu, L. Guo, Colorimetric detection of benzoyl peroxide based on the etching of silver nanoshells of Au@Ag nanorods, Sens. Actuators B Chem. 261 (2018) 379–384, https://doi.org/10.1016/j.snb.2018.01.172.
[41] B. Nikoobakht, M.A. El-Sayed, Preparation and growth mechanism of gold nanorods (NRs) using seed-Mediated growth method, Chem. Mater. 15 (2003) 1957–1962, https://doi.org/10.1021/cm020732l.
[42] M.G. Simic, S.V. Jovanovic, Antioxidation mechanisms of uric acid, J. Am. Chem. Soc. 111 (1989) 5778–5782, https://doi.org/10.1021/ja00197a042.
[43] J. Zeng, S. Fan, C. Zhao, Q. Wang, T. Zhou, X. Chen, Z. Yan, Y. Li, W. Xing, X. Wang, A colorimetric agarose gel for formaldehyde measurement based on nanotechnology involving Tollens reaction, Chem. Commun. 50 (2014) 8121–8123, https://doi.org/10.1039/C4CC00914B.
[44] Y. Wu, P. Jiang, M. Jiang, T.-W. Wang, C.-F. Guo, S.-S. Xie, Z.-L. Wang, The shape evolution of gold seeds and gold@silver core–shell nanostructures, Nanotechnology 20 (2009) 305602, , https://doi.org/10.1088/0957-4484/20/30/305602.
[45] C.-C. Huang, Z. Yang, H.-T. Chang, Synthesis of dumbbell-shaped Au–Ag core-shell nanorods by seed-mediated growth under alkaline conditions, Langmuir 20 (2004) 6089–6092, https://doi.org/10.1021/la048791w.
[46] Y.-F. Huang, K.-M. Huang, H.-T. Chang, Synthesis and characterization of au core–Au–Ag shell nanoparticles from gold seeds: impacts of glycine concentration and pH, J. Colloid Interf. Sci. 301 (2006) 145–154, https://doi.org/10.1016/j.jcis.2006.04.079.
[47] Y. Okuno, K. Nishioka, A. Kiya, N. Nakashima, A. Ishibashi, Y. Niidome, Uniform and controllable preparation of Au–Ag core-shell nanorods using anisotropic silver shell formation on gold nanorods, Nanoscale 2 (2010) 1489, https://doi.org/10.1039/c0nr00130a.
[48] A.C. Moffat, M.D. Osselton, B. Widdop, J. Watts (Eds.), Clarke's Analysis of Drugs and Poisons: In Pharmaceuticals, Body Fluids and Postmortem Material, 4th ed., Pharmaceutical Press, London, 2011.
[49] M. Afzal, P. Minor, J. Begley, M. Bentley, E. Armitage, S. Ghosh, A. Ferguson, Absence of measles-virus genome in inflammatory bowel disease, Lancet 351 (1998) 646–647, https://doi.org/10.1016/S0140-6736(05)78429-4.
[50] G. Chwatko, E. Bald, Determination of cysteine in human plasma by high-performance liquid chromatography and ultraviolet detection after pre-column derivatization with 2-chloro-1-methylpyridinium iodide, Talanta 52 (2000) 509–515, https://doi.org/10.1016/S0039-9140(00)00394-5.
[51] G.D. Baura, Artificial Pancreas, in: G.D. Baura (Ed.), Medical Device Technolnologies, Academic Press, Oxford, 2012, pp. 423–452, , https://doi.org/10.1016/B978-0-12-374976-5.00020-7 ch. 20.